RSC Advances

PAPER

View Article Online
View Journal | View Issue



Cite this: *RSC Adv.*, 2020, **10**, 26874

# A mitochondrial-targetable dual functional near-infrared fluorescent probe to monitor pH and $H_2O_2$ in living cells and mice†

Xueyuan Bi,[a] Yingying Wang,[a] Dandan Wang,[a] Liming Liu,[a] Wen Zhu,[a] Junjie Zhang[b] and Xiaoming Zha *[a]

Received 30th April 2020
Accepted 29th June 2020

DOI: 10.1039/d0ra03905e

rsc.li/rsc-advances

A lower pH level and high hydrogen peroxide ($H_2O_2$) concentration in mitochondria is closely associated with a variety of diseases including cancer and inflammation. Thus, determination of changes in the level of acidic pH and $H_2O_2$ is of great importance and could provide new insights into the key functions under both physiological and pathological conditions. Herein, we present a novel mitochondria-targetable probe **NIR-pH-$H_2O_2$**, as the first near infrared (NIR) fluorescent small molecule, to monitor changes of endogenous pH ($pK_a$ = 6.17) and $H_2O_2$ with high sensitivity, good compatibility and low cytotoxicity. Futhermore, it was successfully employed to monitor pH and $H_2O_2$ in a mouse acute inflammation model. These results demonstrate that **NIR-pH-$H_2O_2$** is a novel bifunctional mitochondrial-targeted NIR probe to sense acidic pH and $H_2O_2$ *in vitro* and *in vivo*, indicating its huge potential for the diagnosis of pH and $H_2O_2$-related diseases.



## Introduction

Intracellular pH is an important parameter in mediating many physiological processes such as cell metabolism, proliferation, apoptosis, ion transport and homeostasis and so on.[1–4] However, abnormal intracellular pH is associated with cellular dysfunctions such as cancer and neurodegenerative disorders.[5,6] Hydrogen peroxide ($H_2O_2$), an important member of reactive oxygen species (ROS) mediates signal cascades involved in redox homeostasis.[7] Substantial evidence has showed that excessive $H_2O_2$ is relevant to serious diseases including cardiovascular disorders, neurodegenerative diseases, cancer and diabetes.[8–13] Wang *et al.* monitored low pH and high $H_2O_2$ in cancer cells, using dual responsive supramolecular polymer by the host–guest interactions of β-CD-hydrazone-DOX and PEG-Fc.[14] Colon cancer cells were extremely sensitive to pH reduction, which naturally cause metabolic stress in the colon lumen, as well as $H_2O_2$ and ionizing radiation.[15] A trend for reduced pH and increased $H_2O_2$ in lower airway inflammation and chronic obstructive pulmonary disease was observed.[16,17] Mitochondria are cellular powerhouses that produce energy through the respiratory chain.[18] Abnormal levels of pH and $H_2O_2$ in the mitochondria are associated with various diseases like cancer, Alzheimer's disease and cardiovascular diseases.[19–22] Thus, determination of mitochondrial changes in pH and level of $H_2O_2$ is of great importance and could provide new insights into the key functions of mitochondria under both physiological and pathological conditions.

Recently, Zhou *et al.* developed a type of two-photon dyes with D–π–A–π–D structure, which possesses near-infrared (NIR) properties, large two-photon absorption cross-section ~160 G and high fluorescence quantum yield ~0.15.[23] The effect of pH on this type of dyes had been studied, pH changes had significant effect on this kind of dyes fluorescence intensity, speculating that in a strong base condition the oxygen-bridge bond could be cut off and in acidic medium recovered easily. To the best of our knowledge, we firstly propose that oxygen-bridge group could be appropriate for the development of acidic pH fluorescent probes. In fluorescent detection field, boric acid group has widely been used as the recognition site toward $H_2O_2$.[24–26] The chemo-selective deprotection of boric acid to phenols provides a useful reaction-based method which detects $H_2O_2$ over other ROS.[27] Additionally, phenylboronic acid ($pK_a$ = 8.70) with relatively weak Lewis acidity is more stability to different pH.[28] Moreover, carbonate as the self-immolative system was applied as a linker of probe which can release $CO_2$ through a 1,6-benzyl elimination.[29,30]

In order to study the biological function or harmful effects of pH and $H_2O_2$ in mitochondria, we present the first mitochondria-immobilized NIR bifunctional fluorescent probe **NIR-pH-$H_2O_2$** for monitoring pH and $H_2O_2$ (Table S1†). As illustrated in Scheme 1, **NIR-pH-$H_2O_2$** consists of **TP-NIR-OH** fluorophore, phenylboronic acid and carbonate linker. The **TP-**

[a]*School of Engineering, China Pharmaceutical University, 639 Longmian Avenue, Nanjing 211198, China*

[b]*School of Pharmacy, China Pharmaceutical University, 639 Longmian Avenue, Nanjing 211198, China. E-mail: xmzha@cpu.edu.cn*

† Electronic supplementary information (ESI) available. See DOI: 10.1039/d0ra03905e

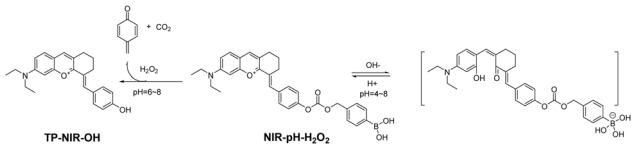


Scheme 1 Proposed reaction mechanism of **NIR-pH-$H_2O_2$** towards pH and $H_2O_2$.

**NIR-OH** fluorophore was predicted to display a NIR fluorescence "off–on" signal response to acidic pH and its positively charged was expected to display mitochondria-specific staining capability. Phenylboronic acid moiety was oxidized by $H_2O_2$ to release $CO_2$ through a 1,6-benzyl elimination, resulting in the recovery of fluorescence. It was successfully applied for image of pH and $H_2O_2$ in mitochondria of live cells and monitoring inflammation in living mice. The present results strongly demonstrated that **NIR-pH-$H_2O_2$** would serve as an excellent bifunctional fluorescent probe to monitor mitochondrial pH and $H_2O_2$ fluctuations in living biological samples.

## Experimental section

### Materials and instruments

Absorption spectra measurements were performed on a Shimadzu UV-vis spectrophotometer, UV-2550. Fluorescent spectra measurements were performed on a Thermo Scientific Lumina fluorescence spectrophotometer. The pH was carried out by a PB 10 digital pH meter. $^1$H NMR (400 MHz) and $^{13}$C NMR (125 MHz) spectra were measured on a Bruker ACF-300 spectrometer (Bruker Corp., Billerica, MA, USA) using TMS as internal reference. Mass spectra was carried on an Agilent 1100 Series (Agilent Technologies, Santa Clara, CA, USA) LC/MSD high performance ion trap mass spectrometer and a Mariner ESI-TOF spectrometer. All starting materials and reagents were purchased from commercial sources and used without further purification. Deionized water was prepared through a water purification system. Fluorescent microscopy imaging was carried out by a confocal laser scanning microscope (CLSM, LSM700, Zeiss, Germany). Fluorescent images of mice were taken by an IVIS Spectrum.

### General procedure for fluorometric analysis

A stock solution of **NIR-pH-$H_2O_2$** (1 mM) was prepared in DMSO. Stock solutions of $H_2O_2$ and other various analytes were prepared with distilled water freshly. A series of standard pH buffer solutions with different values were prepared by the standard procedures. Before absorption and fluorescence spectral measurements, all the resulting solutions were shaken well and incubated for 60 min at room temperature, all fluorescence measurements were executed with the excitation wavelength of 560 nm and the emission wavelength of 680 nm unless other noted.

### The p$K_a$ values of NIR-pH-$H_2O_2$

The p$K_a$ values of **NIR-pH-$H_2O_2$** were calculated using the Henderson–Hasselbalch equation: $\log[(I_{max} - I)/(I - I_{min})] = \text{pH} - \text{p}K_a$. Where $I$ was the observed fluorescence intensity, $I_{max}$ and $I_{min}$ were the corresponding maximum and minimum fluorescence intensity, respectively.[31]

### Cytotoxicity assay and fluorescence imaging toward pH and $H_2O_2$ in living cells

The cytotoxic effect of **NIR-pH-$H_2O_2$** was assessed by the MTT assay. After cells attachment, MCF-7 and Hela cell lines pretreated in medium with **NIR-pH-$H_2O_2$** at different concentrations. 200 μL DMSO was added to each well and shaken for 20 min. The absorbance was measured at 490 nm with a microplate reader (Tecan US, Inc. USA). Cell viability was calculated using the following equation:

$$\text{Cell viability (\%)} = \text{optical density value (treatment group)/optical density value (control group)} \times 100\%.$$

Before imaging, cells were passed and seeded in glass dishes. For labeling, the cells were incubated with 10 μM of **NIR-pH-$H_2O_2$** for the specific incubation time. Then, cells were washed three times with PBS (phosphate buffered saline). Cell images were then recorded using a confocal laser scanning microscope (CLSM, LSM700, Zeiss, Germany) and processed using the ZEN imaging software. Other information is available in the figure captions.

### Animal models and *in vivo* animal studies

Athymic nude mice were purchased from Qinglongshan Animal Breeding Farm (Nanjing, China) for *in vivo* imaging studies. All animal procedures were performed in accordance with the Guidelines for Care and Use of Laboratory Animals of China Pharmaceutical University and the experiments were approved by the Animal Ethics Committee of China Pharmaceutical University.

Before animal imaging, nude mice were given an intraperitoneal injection of lipopolysaccharide (2 mg mL$^{-1}$) in 100 μL PBS for group A. **NIR-pH-$H_2O_2$** (250 μM) in 200 μL buffered solution was injected in the same way for group B. Lipopolysaccharide (2 mg mL$^{-1}$) in 100 μL PBS buffer solution was injected intraperitoneally firstly. After 12 h, **NIR-pH-$H_2O_2$** (250 μM) in 200 μL of buffered solution was injected at the same region for group C. All fluorescence images were acquired with auto exposure (IVIS Spectrum) after incubation for 30 min by using the NIR fluorescence imaging system (excitation wavelength = 560 nm, emission wavelength = 680 nm).[32]

### Synthesis of NIR-pH-$H_2O_2$

The probe **NIR-pH-$H_2O_2$** was synthesized by the procedure shown in Fig. S1.† **TP-NIR-OH** and **B1** was synthesized according to the reported methods.[23,30]

**TP-NIR-OH** (62 mg, 0.2 mmol), compound **B1** (80 mg, 0.2 mmol) and $K_2CO_3$ (65 mg, 0.6 mmol) were dissolved in 5 mL anhydrous DMF under nitrogen. The mixture was allowed to stir at room temperature for 2 h. The solvent was removed under reduced pressure. Then the residue was purified on a silica gel column with $CH_2Cl_2$ to $CH_2Cl_2$/methanol (v/v, 200/1 to 15/1) as eluent to afford **NIR-pH-$H_2O_2$** as black solid (30 mg, 21% yield). $^1$H NMR (500 MHz, DMSO-$d_6$) $\delta$ 8.55 (s, 1H), 8.06 (s, 2H), 8.04 (s, 1H), 7.90 (d, $J$ = 9.5 Hz, 1H), 7.79 (d, $J$ = 7.7 Hz, 2H), 7.67 (d, $J$ = 8.6 Hz, 2H), 7.48–7.46 (m, 1H), 7.38–7.36 (m, 4H), 7.30 (d, $J$ = 1.7 Hz, 1H), 5.25 (s, 2H), 3.68 (m, 4H), 2.90–2.83 (m, 4H), 1.81 (m, 2H), 1.21 (t, $J$ = 6.8 Hz, 6H). $^{13}$C NMR (125 MHz, DMSO-$d_6$) $\delta$ 161.81, 159.16, 156.67, 153.13, 151.66, 149.34, 137.02, 134.82, 134.61, 133.65, 132.67, 132.45, 129.25, 127.66, 123.94, 122.15, 120.02, 119.37, 95.98, 70.51, 70.27, 55.40, 46.21, 40.52, 40.36, 40.19, 40.02, 39.86, 39.69, 39.52, 31.76, 30.88, 29.49, 27.19, 26.99, 22.57, 21.59, 14.42, 12.89. HRMS (ESI): calcd for $C_{32}H_{33}BNO_6^+$ $[M]^+$ $m/z$ 538.2395, found 538.2416. Purity: 98.5% (HPLC).

## Results and discussion

### UV-vis and fluorescence responses to pH

Scheme 2 shows the synthetic route adopted for the preparation of **NIR-pH-$H_2O_2$**, whose structure was further characterized by $^1$H NMR, $^{13}$C NMR and HRMS (Fig. S8–S10†). The fluorescence behaviors of **NIR-pH-$H_2O_2$** (10 μM) towards pH were obtained containing 6% $CH_3CN$ (v/v). As shown in Fig. 1, a significantly large stokes shift of 120 nm was noticed of **NIR-pH-$H_2O_2$** with an absorption maximum ($\lambda_{abs}$) of 560 nm (Fig. 1A) and an emission maximum ($\lambda_{em}$) of 680 nm (Fig. 1B). Both intensity of absorption at 560 nm and fluorescence at 680 nm were dramatically reduced as the value of pH (2.96–9.08) gradually increased (Fig. 1C). Moreover, there is an excellent linear relationship of pH over the range of 4.93 to 7.47 (Fig. 1C inset, $R^2$ = 0.9937). By the nonlinear regression analysis, the p$K_a$ value was calculated to be 6.17, indicating that **NIR-pH-$H_2O_2$** is capable of assessing acidic media. Additionally, the probe shows satisfactory reversibility between pH 4.0 and pH 8.0 (Fig. 1D).

### UV-vis and fluorescence responses to $H_2O_2$

To investigate the interaction between $H_2O_2$ and **NIR-pH-$H_2O_2$**, UV titration was performed (Fig. 2A). The main absorption peak at 560 nm obviously increased with $H_2O_2$ (200 μM). Subsequently, the fluorescence of **NIR-pH-$H_2O_2$** were explored (Fig. 2B). The free probe exhibited a weak fluorescence emission at 680 nm in PBS buffer. However, its fluorescence immediately increased in the presence of $H_2O_2$ (200 μM). This result was consistent with its UV absorption spectrum to $H_2O_2$. As expected, **NIR-pH-$H_2O_2$** is weak-fluorescent (Fig. 2B) in NIR area.

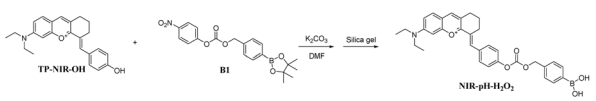


Scheme 2 Synthesis route for NIR-pH-$H_2O_2$.

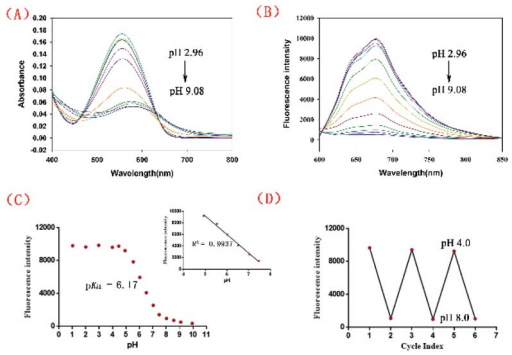


Fig. 1 (A) Absorption and (B) fluorescence emission spectra of NIR-pH-$H_2O_2$ (10 μM) in the phosphate buffer (6% $CH_3CN$) with various pH values. (C) Plot of I 680 *vs.* pH in the range of 1.02 to 9.94. Inset: the linear fitting curve of $I_{680nm}$ *vs.* pH from 4.93 to 7.47. (D) Reversible fluorescence changes of NIR-pH-$H_2O_2$ between pH 4.0 and 8.0 with $\lambda_{ex}$ at 560 nm.

The introduction of $H_2O_2$ could specifically convert the phenylboronic acid unit into an electron-donor-OH group with $CO_2$ released through a 1,6-benzyl elimination, which resulted a significant fluorescence enhancement at 680 nm. A fluorescence titration of **NIR-pH-$H_2O_2$** was carried out to further investigate the quantitative relationship between **NIR-pH-$H_2O_2$** and $H_2O_2$. With the increasing of $H_2O_2$, its fluorescence intensity at 680 nm gradually increased (Fig. 2C and D). When the concentration increased to 130 μM, the fluorescence almost kept stable. In addition, the fluorescence intensity of **NIR-pH-$H_2O_2$** showed an excellent linear relationship with the $H_2O_2$ concentration ($R^2$ = 0.9968 Fig. 2D inset). The detection limit (utilizing the $3\sigma/k$ method) for $H_2O_2$ was determined 2.097 μM. which was enough for direct image of intracellular $H_2O_2$ as its concentrations are usually in sub-micromolar range.[25] To ensure whether **NIR-pH-$H_2O_2$** could be applied for real-time detection, the kinetic experiments towards $H_2O_2$ were explored (Fig. S1†). It was displayed that the detection process balanced within 30 minutes, after adding $H_2O_2$ to the probe

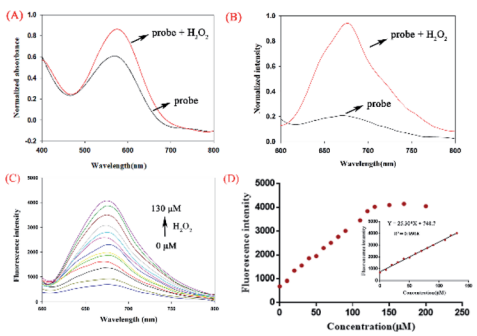


Fig. 2 Absorption (A) and fluorescence (B) spectra of NIR-pH-$H_2O_2$ (10 μM) in PBS buffer (6% $CH_3CN$). (C) Fluorescence spectra of NIR-pH-$H_2O_2$ (10 μM) in the presence of various amounts of $H_2O_2$ (0–130 μM) in PBS buffer. (D) The curve was plotted with fluorescence intensity *vs.* $H_2O_2$ concentration (0–200 μM) inset: linear relationship between fluorescence intensity of NIR-pH-$H_2O_2$ and $H_2O_2$ concentration (0–130 μM) at 680 nm ($\lambda_{ex}$ = 560 nm).

solution and a small quantity of enhancement was observed within the next 20 minutes.

### Sensitivity detection

Subsequently, the fluorescence specificity of **NIR-pH-$H_2O_2$** was examined over various other species. As shown in Fig. 3, the fluorescence intensity at 680 nm of $H^+$ and $H_2O_2$ are stronger than the other tested analytes in the phosphate buffer (6% $CH_3CN$) indicating that **NIR-pH-$H_2O_2$** was sensitive to protonic acid (pH = 4) and $H_2O_2$. These unique properties enable it to be feasible to accurately measure intracellular pH and $H_2O_2$ with high selectivity.

### The response between NIR-pH-$H_2O_2$ and $H_2O_2$ at different pH

It was of great significance to know the response between **NIR-pH-$H_2O_2$** and $H_2O_2$ at different pH levels. The fluorescence intensity of **NIR-pH-$H_2O_2$** and **NIR-pH-$H_2O_2$** + $H_2O_2$ was then measured in PBS buffer from pH 1 to 10, respectively (Fig. S2†). It was found that fluorescence intensity of **NIR-pH-$H_2O_2$** can increase upon the addition of $H_2O_2$ in the pH (1–10) range and the most obvious increase toward $H_2O_2$ could be observed from pH 6.0 to 8.0, indicating it can be applied in most living organisms (the physiological environment pH = 7.4).

### Mechanism studies

The phenylboronic acid group in **NIR-pH-$H_2O_2$** was the reaction site with $H_2O_2$ (Scheme 1). The starting material **TP-NIR-OH** was produced through a 1,6-benzyl elimination. The result of the electrospray ionization mass spectrometry (ESI-MS) confirmed the mechanism of this reaction. Addition of $H_2O_2$ in the **NIR-pH-$H_2O_2$** solution resulted in a new peak at 360.19578 which correspond to **TP-NIR-OH** $[M + H^+]$ (Fig. S12†). The same results were also shown in the HPLC analysis (Fig. S13†). Thus, the results were in line with the proposed mechanism.

### Cytotoxicity and cell mitochondria-targeting specificity of NIR-pH-$H_2O_2$

Before intracellular experiments, a standard MTT assay of MCF-7 and Hela cell lines were carried out to evaluate the biocompatibility of **NIR-pH-$H_2O_2$**. When the probe concentration reached 50 μM, **NIR-pH-$H_2O_2$** displayed negligible cell toxicity since nearly 80% of MCF-7 cells (Fig. S3A†) and 85% of HeLa cells (Fig. S3B†) survived and could be applied to biological cells. To confirm the presumed mitochondria-targeting specificity of **NIR-pH-$H_2O_2$**, the colocalization experiments were performed in MCF-7 cells using Mito Tracker Green (a commercial mitochondria-targeting dye). As expected, the fluorescence image produced using **NIR-pH-$H_2O_2$** (Fig. 4A) overlaps with that obtained using Mito Tracker Green (Fig. 4B), the fluorescence distribution of **NIR-pH-$H_2O_2$** overlaps well with that of Mito Green (Pearson' s coefficient, 0.90; Fig. S4, parts D and E†). In summary, these data proved that **NIR-pH-$H_2O_2$** was a good mitochondria-targeted fluorescent probe.

### Cell imaging of NIR-pH-$H_2O_2$ for pH and $H_2O_2$

To explore capacity of **NIR-pH-$H_2O_2$** for living cell fluorescence imaging of pH changes, MCF-7 cells and Hela cells were evaluated using the confocal fluorescence imaging. The fluorescence intensity of **NIR-pH-$H_2O_2$** in MCF-7 cells (Fig. 5A) and Hela cells (Fig. S4A†) gradually decreased with increasing pH over the range of pH 5.08 to 7.84, indicated that **NIR-pH-$H_2O_2$** could be applied for the detection of pH in living cells. We then employed **NIR-pH-$H_2O_2$** to determine the pH change in mitochondria with a rapamycin model.[32] Rapamycin, a widely used macrolide antibiotic, induces mitophagy in a variety of cell types and acidification of mitochondria has been observed during the mitophagy.[33–35] MCF-7 cells and HeLa cells were treated with **NIR-pH-$H_2O_2$** and rapamycin for 1 h then fluorescence images were recorded. As expected, the merged images of the rapamycin-treated MCF-7 cells (Fig. 5B) and HeLa cells (Fig. S4B†) exhibit more obvious colour change, which is ascribed to the rapamycin-induced generation of mitophagy and decrease of the mitochondrial pH.

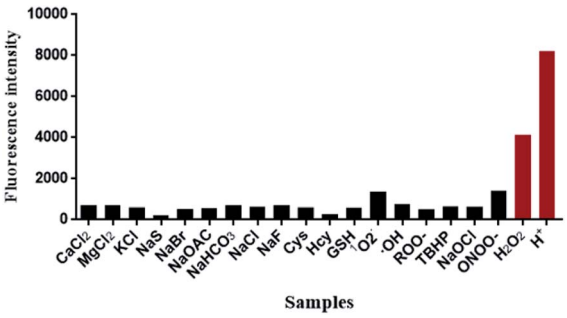


Fig. 3 Fluorescence response of **NIR-pH-$H_2O_2$** (10 μM) upon addition of various analytes (200 μM: $CaCl_2$; $MgCl_2$; KCl; NaS; NaBr; NaOAC; $NaHCO_3$; NaCl; NaF; Cys; Hcy; GSH; $^1O_2$; ·OH; ROO·; TBHP; NaOCl; ONOO−; $H_2O_2$ and $H^+$ (pH = 4) in PBS buffer (6% $CH_3CN$)).

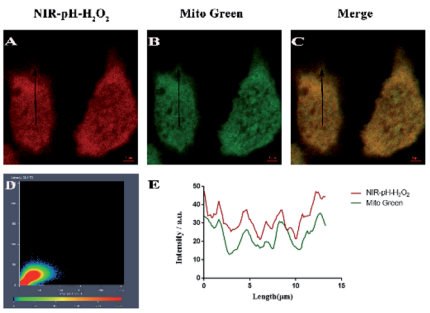


Fig. 4 Colocalization experiments involving **NIR-pH-$H_2O_2$** and Mito Tracker Green (MTG) in MCF-7 cells. The cells were incubated with **NIR-pH-$H_2O_2$** (10 μM) and MTG (5 μM) for 30 min at 37 °C, followed by treatment with 200 μM $H_2O_2$ for 30 min at 37 °C. Images for **NIR-pH-$H_2O_2$** (A) and MTG (B) were then recorded using excitation wavelengths of 555 nm and 485 nm, and band-path emission filters at 680 nm and 514 nm, respectively. Panels (C) shows a merged image of (A) and (B). (D) Intensity scatter plot of channels 1 and 2. (E) Intensity correlation plot of **NIR-pH-$H_2O_2$** and MTG (Pearson's coefficient 0.90). Scale bar: 2 μm.

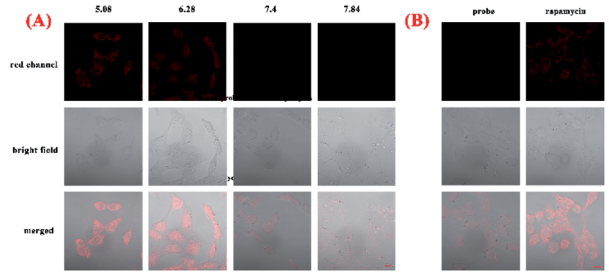


Fig. 5 (A) Fluorescent microscopic images of MCF-7 cells with **NIR-pH-$H_2O_2$**. Incubated cells with 10 μL of **NIR-pH-$H_2O_2$** (10 μM) under the pH 5.08, 6.28, 7.4, 7.84 and (B) rapamycin (10 μM) of the culture medium for 30 min and observed under the microscope ($\lambda_{ex}$ = 555 nm, $\lambda_{em}$ = 680 nm for the red channel). Scale bar: 10 μm.

Next, we investigated the fluorescence imaging of **NIR-pH-$H_2O_2$** for $H_2O_2$ in MCF-7 (Fig. 6a–d) cells and Hela cells (Fig. S5a–d†). After incubation with probe **NIR-pH-$H_2O_2$** for 30 min at 37 °C, almost no fluorescence could be observed for non-$H_2O_2$. However, fluorescence intensities became increased after treated with increased exogenous $H_2O_2$. The results were consistent with our previous results of fluorescence spectra, showing that **NIR-pH-$H_2O_2$** could be used for $H_2O_2$ detection in living cells. Next, application of **NIR-pH-$H_2O_2$** to visualize endogenous $H_2O_2$ in MCF-7 cells and Hela cells by confocal fluorescence microscopy. To induce acute endogenous $H_2O_2$ production, the nonspecific protein kinase C activator phorbol myristate acetate (PMA; 200 ng $mL^{-1}$) was co-incubated with **NIR-pH-$H_2O_2$** for 30 min, followed by confocal imaging.[36,37] Fluorescence intensity of **NIR-pH-$H_2O_2$** sharply enhanced due to PMA treatment triggered an oxidative burst in for MCF-7 cells (Fig. 6e) and Hela cells (Fig. S5e†) compared with the control group. These results indicate the capability of **NIR-pH-$H_2O_2$** in determining the endogenous changes of $H_2O_2$ in living cells. Dynamic fluorescence imaging for **NIR-pH-$H_2O_2$** was further conducted. After incubated with exogenous $H_2O_2$ and probe **NIR-pH-$H_2O_2$** in MCF-7 (Fig. S6†) and Hela cell lines (Fig. S7†), red fluorescence was enhanced gradually after incubated for 0 min, 10 min, 20 min and 30 min. The results were consistent with our previous results of fluorescence spectra.

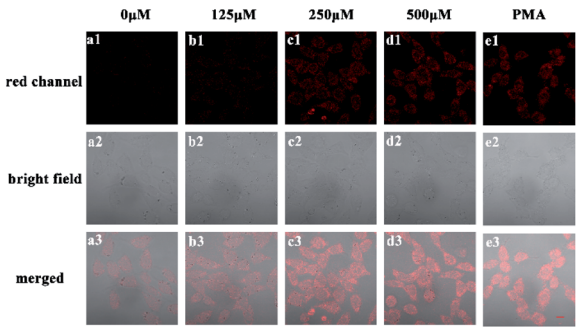


Fig. 6 Fluorescence images of **NIR-pH-$H_2O_2$** (10 μM) with various concentrations of $H_2O_2$ solution and PMA ($\lambda_{ex}$ = 555 nm, $\lambda_{em}$ = 680 nm for the red channel). The MCF-7 was treated with **NIR-pH-$H_2O_2$** and different concentration of $H_2O_2$ and PMA for 30 min. Scale bar: 10 μm.

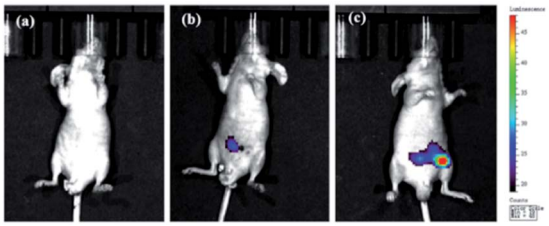


Fig. 7 *In vivo* fluorescence images in the peritoneal cavity of mice injected with **NIR-pH-$H_2O_2$** during LPS-induced inflammatory response. (a) Only LPS was injected for control. (b) Saline was injected in the peritoneal cavity of mouse, followed by injection of **NIR-pH-$H_2O_2$** (50 μM). (c) LPS was in-jected into the peritoneal cavity of the mouse, followed by injection with **NIR-pH-$H_2O_2$** (50 μM). The mice were imaged with an excitation filter at 560 nm and emission filter at 680 nm.

### Fluorescence imaging of NIR-pH-$H_2O_2$ in mice

Having achieved successful cell imaging with **NIR-pH-$H_2O_2$**, a further exploratory effort was made to determine whether it would be competent of fluorescence imaging *in vivo* and reflect occurrence of biological processes induced by exogenous stimulation. Since abdominal inflammation induced by lipopolysaccharide (LPS) could cause changes of pH and overproduction of hydrogen peroxide,[38–40] we investigated the application of **NIR-pH-$H_2O_2$** to visualize fluorescence changes in an abdominal inflammation mouse model induced by LPS. As shown in Fig. 7b, the mouse treated with saline and **NIR-pH-$H_2O_2$** exhibited low fluorescence intensity. However, the fluorescence intensity in the mouse treated with LPS and **NIR-pH-$H_2O_2$** changed evidently (Fig. 7c), which was attributed to that the inflammatory response could reduce the local pH and increased the level of $H_2O_2$. As the control, the mouse treated with LPS but no **NIR-pH-$H_2O_2$** injection showed no fluorescence (Fig. 7a). Therefore, these results demonstrate that **NIR-pH-$H_2O_2$** is a prominent fluorescent probe for imaging inflammation *in vivo*.

## Conclusions

In summary, we firstly reported a novel "off–on" dual functional NIR fluorescent probe **NIR-pH-$H_2O_2$** to monitor pH and $H_2O_2$ *in vitro* and *in vivo*. The cellular assay confirmed that **NIR-pH-$H_2O_2$** is co-localized in mitochondria with low cytotoxicity. Furthermore, the probe shows excellent pH sensitivity, good response to $H_2O_2$, and successful imaging of pH and $H_2O_2$ in mice inflammation model induced by LPS. Mitochondria acidification is seen during the mitophagy. Abnormal levels of mitophagy and $H_2O_2$ are associated with various pathological conditions such as cancer, inflammation and neurodegenerative diseases. On the basis of these results, we envision that **NIR-pH-$H_2O_2$** could be employed to understand the roles of reduced pH and increased $H_2O_2$ in pathological conditions and further

for the pH and $H_2O_2$ related diseases diagnosis and real-time monitoring.

## Conflicts of interest

There are no conflicts to declare.

## Acknowledgements

This work was supported by the National Natural Science Foundation of China (81973187), "Six Talent Peaks" Project of Jiangsu Province (2016-YY-042), National Key Research and Development Program (2017YFC0107700), "Double First-Class" University project (CPU2018GY24, CPU2018GY38) and National Found for Fostering Talents of Basic Science (NFFTBS, No. J1310032).

## Notes and references

1 W. J. Waddell and R. G. Bates, *Physiol. Rev.*, 1969, **49**, 285–329.
2 R. A. Gottlieb and A. Dosanjh, *Proc. Natl. Acad. Sci. U. S. A.*, 1996, **93**, 3587–3591.
3 D. Pérez-Sala, D. Collado-Escobar and F. Mollinedo, *J. Biol. Chem.*, 1995, **270**, 6235–6242.
4 P. Donoso, M. Beltrán and C. Hidalgo, *Biochemistry*, 1996, **35**, 13419–13425.
5 K. Ji, L. Mayernik, K. Moin and B. F. Sloane, *Cancer Metastasis Rev.*, 2019, **38**, 103–112.
6 J. M. Holopainen, J. Saarikoski, P. K. Kinnunen and I. Järvelä, *Eur. J. Biochem.*, 2001, **268**, 5851–5856.
7 T. Finkel, M. Serrano and M. A. Blasco, *Nature*, 2007, **448**, 767–774.
8 C. H. Byon, J. M. Heath and Y. Chen, *Redox Biol.*, 2016, **9**, 244–253.
9 E. Niedzielska, I. Smaga, M. Gawlik, A. Moniczewski, P. Stankowicz, J. Pera and M. Filip, *Mol. Neurobiol.*, 2016, **53**, 4094–4125.
10 M. P. Murphy, A. Holmgren, N.-G. Larsson, B. Halliwell, C. J. Chang, B. Kalyanaraman, S. G. Rhee, P. J. Thornalley, L. Partridge, D. Gems, T. Nyström, V. Belousov, P. T. Schumacker and C. C. Winterbourn, *Cell Metab.*, 2011, **13**, 361–366.
11 L. Park, P. Zhou, R. Pitstick, C. Capone, J. Anrather, E. H. Norris, L. Younkin, S. Younkin, G. Carlson, B. S. McEwen and C. Iadecola, *Proc. Natl. Acad. Sci. U. S. A.*, 2008, **105**, 1347–1352.
12 N. Houstis, E. D. Rosen and E. S. Lander, *Nature*, 2006, **440**, 944–948.
13 C. Behl, *Cell*, 1994, **77**, 817–827.
14 Y. Wang, H. Wang, Y. Chen, X. Liu, Q. Jin and J. Ji, *Colloids Surf., B*, 2014, **121**, 189–195.
15 M. S. Moon, E. W. Cho, H. S. Byun, I. L. Jung and I. G. Kim, *Arch. Biochem. Biophys.*, 2004, **430**, 229–236.
16 M. Duz, A. G. Whittaker, S. Love, T. D. H. Parkin and K. J. Hughes, *Res. Vet. Sci.*, 2009, **87**, 307–312.
17 K. Murata, K. Fujimoto, Y. Kitaguchi, T. Horiuchi, K. Kubo and T. Honda, *Chronic Obstr. Pulm. Dis.*, 2014, **11**, 81–87.
18 L. Ernster and G. Schatz, *J. Cell Biol.*, 1981, **91**, 227s–255s.
19 L. Jiang, L. Li, X. He, Q. Yi, B. He, J. Cao, W. Pan and Z. Gu, *Biomaterials*, 2015, **52**, 126–139.
20 G. E. Weitsman, R. Koren, E. Zuck, C. Rotem, U. A. Liberman and A. Ravid, *Free Radical Biol. Med.*, 2005, **39**, 266–278.
21 I. A. Pomytkin, *Curr. Neuropharmacol.*, 2012, **10**, 311–320.
22 J. Marx, *Science*, 2005, **307**, 334–335.
23 L. Zhou, D. Lu, Q. Wang, S. Liu, Q. Lin and H. Sun, *Biosens. Bioelectron.*, 2017, **91**, 699–705.
24 K. Liu, H. Shang, X. Kong, M. Ren, J.-Y. Wang, Y. Liu and W. Lin, *Biomaterials*, 2016, **100**, 162–171.
25 G. C. van de Bittner, E. A. Dubikovskaya, C. R. Bertozzi and C. J. Chang, *Proc. Natl. Acad. Sci. U. S. A.*, 2010, **107**, 21316–21321.
26 X.-Q. Zhan, B.-Y. Su, H. Zheng and J.-H. Yan, *Anal. Chim. Acta*, 2010, **658**, 175–179.
27 L. Zhou, H. Ding, W. Zhao and S. Hu, *Spectrochim. Acta, Part A*, 2019, **206**, 529–534.
28 Z. Guo, I. Shin and J. Yoon, *Chem. Commun.*, 2012, **48**, 5956–5967.
29 H. Y. Lee, X. Jiang and D. Lee, *Org. Lett.*, 2009, **11**, 2065–2068.
30 P. Wang, K. Wang and Y. Gu, *Sens. Actuators, B*, 2016, **228**, 174–179.
31 B. Dong, X. Song, C. Wang, X. Kong, Y. Tang and W. Lin, *Anal. Chem.*, 2016, **88**, 4085–4091.
32 X. Li, Y. Hu, X. Li and H. Ma, *Anal. Chem.*, 2019, **91**, 11409–11416.
33 Y.-Q. Shen, A. Guerra-Librero, B. I. Fernandez-Gil, J. Florido, S. García-López, L. Martinez-Ruiz, M. Mendivil-Perez, V. Soto-Mercado, D. Acuña-Castroviejo, H. Ortega-Arellano, V. Carriel, M. E. Diaz-Casado, R. J. Reiter, I. Rusanova, A. Nieto, L. C. López and G. Escames, *J. Pineal Res.*, 2018, **64**, 1–18.
34 F. Hu, X. Cai, P. N. Manghnani, Kenry, W. Wu and B. Liu, *Chem. Sci.*, 2018, **9**, 2756–2761.
35 H. Yuan, H. Cho, H. H. Chen, M. Panagia, D. E. Sosnovik and L. Josephson, *Chem. Commun.*, 2013, **49**, 10361–10363.
36 S. Ye, J. J. Hu and D. Yang, *Angew. Chem., Int. Ed. Engl.*, 2018, **57**, 10173–10177.
37 P. Wu, Z. Cai, Y. Gao, H. Zhang and C. Cai, *Chem. Commun.*, 2011, **47**, 11327–11329.
38 Y. Li, Y. Wang, S. Yang, Y. Zhao, L. Yuan, J. Zheng and R. Yang, *Anal. Chem.*, 2015, **87**, 2495–2503.
39 N. Karton-Lifshin, E. Segal, L. Omer, M. Portnoy, R. Satchi-Fainaro and D. Shabat, *J. Am. Chem. Soc.*, 2011, **133**, 10960–10965.
40 L. Fan, X. Wang, J. Ge, F. Li, C. Zhang, B. Lin, S. Shuang and C. Dong, *Chem. Commun.*, 2019, **55**, 6685–6688.